Occult progression by *Apc*-deficient intestinal crypts as a target for chemoprevention

Jared M.Fischer, Arnout G.Schepers[1,2], Hans Clevers[2], Darryl Shibata[3] and R.Michael Liskay*

Department of Molecular and Medical Genetics, Oregon Health and Science University, Portland, OR 97239, USA, [1]Harvard-MIT Division of Health Sciences and Technology, Massachusetts Institute of Technology, Cambridge, MA 02139, USA, [2]Hubrecht Institute, Developmental Biology and Stem Cell Research, KNAW and University Medical Center Utrecht, Uppsalaan 8, 3584 CT Utrecht, The Netherlands and [3]Department of Pathology, Norris Cancer Center, Keck School of Medicine, University of Southern California, Los Angeles, CA 90033, USA

*To whom correspondence should be addressed. Tel: +503 494 4346
Fax: +503 494 6886
Email: liskaym@ohsu.edu

Although *Apc* mutation is widely considered an initiating event in colorectal cancer, little is known about the earliest stages of tumorigenesis following sporadic *Apc* loss. Therefore, we have utilized a novel mouse model that facilitates the sporadic inactivation of *Apc* via frameshift reversion of *Cre* in single, isolated cells and subsequently tracks the fates of *Apc*-deficient intestinal cells. Our results suggest that consistent with *Apc* being a 'gatekeeper', loss of *Apc* early in life during intestinal growth leads to adenomas or increased crypt fission, manifested by fields of mutant but otherwise normal-appearing crypts. In contrast, *Apc* loss occurring later in life has minimal consequences, with mutant crypts being less prone to either increased crypt fission or adenoma formation. Using the stem cell-specific *Lgr5-CreER* mouse, we generated different sized fields of *Apc*-deficient crypts via independent recombination events and found that field size correlates with progression to adenoma. To evaluate this early stage prior to adenoma formation as a therapeutic target, we examined the chemopreventive effects of sulindac on *Apc*-deficient occult crypt fission. We found that sulindac treatment started early in life inhibits the morphologically occult spread of *Apc*-deficient crypts and thus reduces adenoma numbers. Taken together these results suggest that: (i) earlier *Apc* loss promotes increased crypt fission, (ii) a field of *Apc*-deficient crypts, which can form via occult crypt fission or independent neighboring events, is an important intermediate between loss of *Apc* and adenoma formation and (iii) normal-appearing *Apc*-deficient crypts are potential unappreciated targets for cancer screening and chemoprevention.

Introduction

The prevailing dogma of solid tumor progression is that cancer results from the stepwise accumulation of multiple mutations beginning within a single cell (1). In colorectal cancer, the adenomatous polyposis coli protein is frequently mutated in the earliest adenomas (1) and is the most commonly mutated gene in colorectal cancer (2). However, little is known about the earliest stages of tumor initiation following *Apc* loss, in particular when loss occurs in isolated stem cells in an otherwise wild-type intestine. Mutation in a single stem cell alone may be insufficient to confer a tumorigenic phenotype and the local environment may play a modifying role by creating a field effect (3,4). The resulting numerical increase in mutant progeny will both raise the odds of further alteration and form a field of adjacent mutant crypts that could enhance tumorigenesis (5). Field effects have been reported for genes such as *p53* in esophageal cancer (6), ulcerative colitis-associated neoplasia (7) and *Cdh3* in colorectal cancer (8). Here, we report for the first time evidence for field effects and occult crypt fission involving a strong tumor initiator, specifically the *Apc*

gene, and how sulindac can inhibit the *Apc*-deficient crypt fission advantage, thereby reducing adenoma number.

A prevalent view is that *Apc* loss in intestinal crypt stem cells is sufficient for adenoma formation (9,10). However, our previous studies in which we examined the effects of *Apc* loss in single crypts surrounded by tissue expressing wild-type levels of *Apc* demonstrated a form of phenotypic plasticity. Namely, following *Apc* loss, adenoma formation could ensue, but the majority of *Apc*-deficient intestinal crypts retained a normal phenotype with increased clonal expansion (11). In both cases (adenoma formation or field formation), *Apc* loss functions as a gatekeeper mutation with net increases in *Apc*-mutant cells (12). Interestingly, a significant fraction of the morphologically normal *Apc*-deficient crypts exhibited a growth advantage resulting in clonal expansion and a field of mutant crypts, thus raising the possibility that crypt fission leading to an occult, horizontal spread of mutations is an important intermediate during tumorigenesis.

Here, we first show that the timing of *Apc* loss can affect field formation by strongly influencing the crypt fission advantage of *Apc*-deficient crypts, with later *Apc* loss resulting in decreased mutant field size and adenoma formation. Next, using the intestinal stem cell-specific Cre, *Lgr5-CreER* system (13,14), we generate different sized fields of *Apc*-deficient crypts and polyclonal adenomas, further substantiating that an expanded *Apc*-deficient field is important for adenoma formation (5,15,16). Finally, we demonstrate that the non-steroidal anti-inflammatory drug (NSAID) sulindac can act as a chemopreventive by inhibiting the *Apc*-deficient occult crypt fission that appears to precede subsequent adenoma formation. Based on these findings, we suggest that: (i) isolated *Apc*-deficient crypts are not highly prone to tumorigenesis, whereas a field of *Apc*-deficient crypts formed by either occult crypt fission or independent neighboring events creates a local environment that is highly conducive to adenoma formation and (ii) minimizing *Apc*-deficient occult crypt fission is a previously unappreciated mechanism of chemoprevention.

Materials and methods

Mice

Pms2cre; *ApcCKO/CKO*; *R26R* mice were generated by interbreeding *Pms2cre/+*; *R26R* mice with *ApcCKO* (17) mice. The *R26R* (*Rosa26 Reporter* mice with *lox-stop-lox LacZ, YFP* or *Confetti*) allele was used (18,19). Mice were housed in a specific pathogen-free High-efficiency particulate air filtered room and were fed a diet of Purina PicoLab Rodent Diet 20. The *R26R* and *Lgr5-CreER* (13) mouse strains were obtained from the Jackson Laboratory (Bar Harbor, ME). Tamoxifen (Sigma) was prepared in sunflower seed oil (Sigma) at a concentration of 10 mg/ml or 1 mg/ml. Two hundred microliters of the tamoxifen solution was intraperitoneally injected once into mice at the specified age. All experiments were approved by the Institutional Animal Care and Use Committee at Oregon Health and Science University. Genotyping was performed as described previously (11) and as described in the supplementary methods, available at *Carcinogenesis* Online. *Lgr5-CreER*; *Apc580S/580S*; *R26R-Confetti* mice were generated and treated as described previously (14). Intestinal organoids were cultured as described previously (20).

Sulindac treatment

Sulindac was administered at different time points through the drinking water and continued until time of sacrifice. The sulindac solution comprised 180 mg/l of sulindac and 4 mM sodium phosphate dibasic in distilled water (pH ~7.4).

Scoring of β-gal+ foci in wholemount intestine

β-gal staining was performed and scored as described previously (11). Nearby β-gal+ foci were considered independent if not arising from the same crypt and surrounded by non-staining crypts. Adenomas, which involve multiple villi, and microadenomas involving a single villus were scored in wholemount and cross sections. We concentrated on the proximal small intestine for β-gal+ foci counts because of inefficient recombination of the Cre reporter in the distal small intestine, as reported previously (21,22). The rate of *cre* reversion was determined by counting the number of colonies with β-gal+ cells versus those without, as described previously (23).

Results

Pms2^cre^ system for fate mapping of mutant intestinal stem cells

To better understand the fates of normal and mutant intestinal cells, we developed the *Pms2^cre^* mouse system that features an out-of-frame *cre* allele to stochastically recombine floxed target genes and the marker gene, β-gal (Figure 1A) (21). This system enables not only the monitoring of tumor formation following stochastic genetic manipulations but also facilitates the tracking of normal or mutant stem cell fates. Replication slippage into frame is a function of cell division (DNA replication), and therefore Cre activation can occur any time after conception. Whereas *Cre* reversion will occur most often in any dividing cell, we stress that only the products of reversion events that take place in either intestinal stem cells (regardless of their position within the crypt) or long-lived progenitors will persist. Finally, we are able to alter the overall timing of *Cre* reversion by modulating the mismatch repair status, such that there is either a high frequency [*Pms2^cre/cre^*, mismatch repair (MMR)-deficient background] or low frequency (*Pms2^cre/+^*, MMR-proficient background) of *Cre* reversion.

Because *Cre* reversion rates are low (~1 in 700 cell divisions in *Pms2^cre/cre^* mouse embryonic fibroblasts), Cre activation overwhelmingly occurs in isolated cells. In *Pms2^cre^* mice carrying a *lox-stop-lox* β-gal allele (*R26R*), clonal patches composed of different numbers of β-gal⁺ crypts/villi are observed. Each β-gal⁺ focus should represent a single *Cre* reversion and is classified by size as either small (1–3 villi), medium (4–9 villi) or large (10+ villi per focus). The different sized foci reflect the normal process of crypt fission that takes place during growth and development of the intestine (Figure 1B–E and Supplementary Figure 1A–D, available at *Carcinogenesis* Online). We directly compared *Pms2^cre/cre^* intestines with *Pms2^cre/+^* intestines, in which *Cre* reversion occurs at a ~50-fold lower rate than in *Pms2^cre/cre^* mice (Figure 2A and B). Because clonal expansion via crypt fission is in part a function of the timing of *Cre* reversion, we predicted that fewer and smaller β-gal⁺ patches should be observed in *Pms2^cre/+^* mice. Consistent with this prediction, the lower reversion rate of *Pms2^cre/+^*; *R26R* mice results in a slower accumulation of reversion events with age (Supplementary Figure 2, available at *Carcinogenesis* Online). As a control, we examined the intestines of 6 *Pms2^+/+^*; *R26R* mice and saw no β-gal⁺ foci, as expected for mice without a *Cre* gene. Therefore, the pattern of β-gal⁺ crypts in either *Pms2^cre/cre^*; *R26R* or *Pms2^cre/+^*; *R26R* mice provides a baseline of how individual stem cells normally form clonal patches throughout life. Depending on the constellation of the *Cre*-target alleles, we can measure not only whether
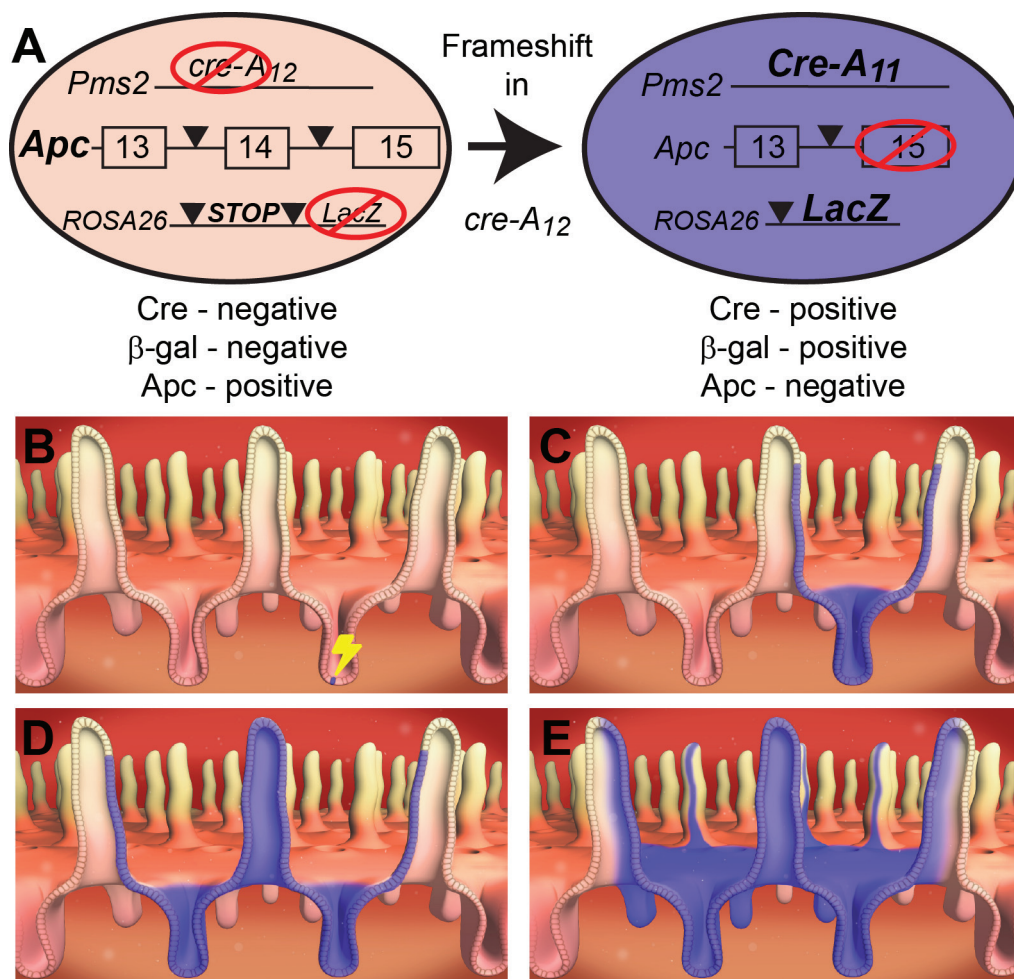

Fig. 1. Progression, following *Cre* reversion, of a β-gal⁺ stem cell to a field of β-gal⁺ crypts. (**A**) Diagram summarizing the *Pms2^cre^* mouse system combined with a conditional *Apc* allele. An out-of-frame *cre* gene is located at the *Pms2* locus. Upon frameshift mutation within the mononucleotide repeat (A12), Cre protein becomes active and recombines the conditional target allele *Apc* and the reporter allele *LacZ*. (**B**) Cre reversion occurs stochastically at low frequency, resulting in a single *Apc*-deficient β-gal⁺ cell within a crypt. Only Cre activation in a stem cell will have the chance to spread throughout the crypt. (**C**) The end product of crypt succession by a single β-gal⁺ stem cell, namely, a monoclonal, β-gal⁺ crypt. (**D**) The end product of crypt fission of the monoclonal, β-gal⁺ crypt producing a pair of neighboring, *Apc*-deficient β-gal⁺ crypts. (**E**) The consequence of continued crypt fission resulting in a field of *Apc*-deficient β-gal⁺ crypts.
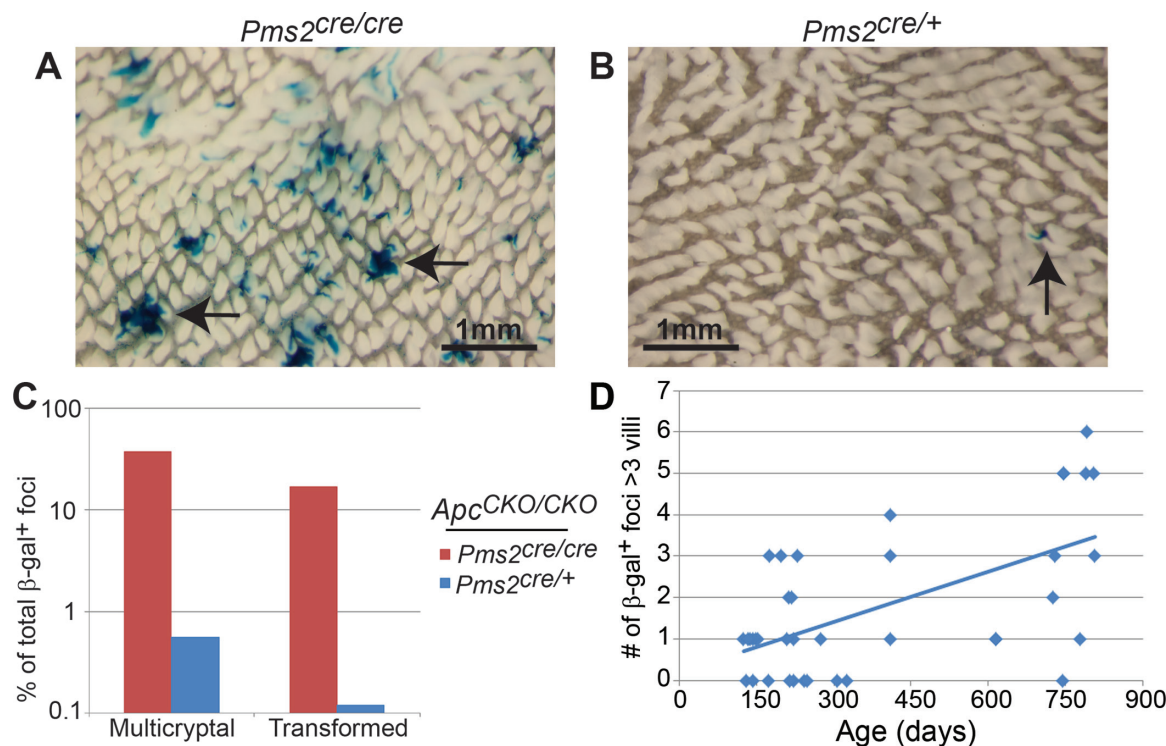
Fig. 2. β-gal⁺ foci number, crypt fission and adenoma formation in *Pms2^cre/cre* and *Pms2^cre/+* intestines. Wholemount images of the proximal small intestine from a *Pms2^cre/cre* (**A**) and *Pms2^cre/+* (**B**) mouse. Arrows show multicryptal β-gal⁺ foci in (A) and a single β-gal⁺ focus in (B). Note the difference in both number and size of β-gal⁺ foci between *Pms2^cre/cre* and *Pms2^cre/+* intestines. (**C**) *Pms2^cre/cre*; *Apc^CKO/CKO* intestines have a higher percentage of normal-appearing multicryptal β-gal⁺ foci and transformed β-gal⁺ foci compared with *Pms2^cre/+*; *Apc^CKO/CKO* intestines. The percentage of transformed β-gal⁺ foci was determined by scoring frozen sections counterstained with nuclear fast red. (**D**) The number of β-gal⁺ foci containing more than three villi results in a linear regression of $y = 0.004x + 0.2$, which is a statistically significant increase with age ($P < 0.001$). The number of β-gal⁺ foci containing more than three villi was determined via wholemount.

mutant intestinal stem cells progress to tumors but also whether mutant cells have undergone altered crypt succession, indicated by the number of β-gal⁺ foci, and/or altered crypt fission, indicated by the size of β-gal⁺ foci.

In contrast to early loss, Apc loss later in life is not conducive to either increased crypt fission or adenoma formation

We previously reported that *Pms2^cre/cre*; *Apc^CKO/CKO* mice exhibited an increase in the size of β-gal⁺ foci compared with *Pms2^cre/cre*; *Apc^+/+* mice, with only a minority (<20%) of *Apc* loss events resulting in either a microadenoma or adenoma. In fact, >80% of β-gal⁺; *Apc^−/−* foci retained a normal phenotype, including normal levels and cellular distribution of β-catenin [11]. While our studies were concentrated on the proximal small intestine, we observed a similar increase in the proportion of larger *Apc*-deficient foci in the medial and distal small intestines of *Pms2^cre/cre* mice (Supplementary Figure 3, available at *Carcinogenesis* Online). We also cultured crypts from *Pms2^cre/cre*; *Apc^CKO/CKO* intestine and found that recombined β-gal⁺ cells can contribute to normal-appearing portions of organoids or cysts typical of an adenoma [20,24] (Supplementary Figure 4, available at *Carcinogenesis* Online). Furthermore, we found that somatic loss of a single *Apc* allele in *Pms2^cre/cre*; *Apc^CKO/+* mice did not increase the number of larger β-gal⁺ foci when compared with *Pms2^cre/cre*; *Apc^+/+* mice, showing that only complete loss of *Apc* function results in increased field size [11] (Supplementary Figure 5, available at *Carcinogenesis* Online). We also compared the number of β-gal⁺ foci with the fraction of β-gal⁺ foci that occupied more than one crypt (multicryptal) and found that >75% of the multicryptal β-gal⁺ foci cannot be explained by independent, neighboring events (Supplementary Table 1, available at *Carcinogenesis* Online). Overall, these results illustrate morphologic phenotypic plasticity of *Apc*-deficient crypts because early *Apc* loss increases clonal expansion (crypt fission) without necessarily resulting in visible adenoma formation.

In contrast to results with *Pms2^cre/cre* mice, we found that conditional alteration of *Apc* in *Pms2^cre/+* mice results in significantly less subsequent crypt clonal expansion and adenoma formation (Figure 2C). Less than 1% of the β-gal⁺ foci in the *Pms2^cre/+*; *Apc^CKO/CKO* mice occupied multiple crypts, starkly different from the 24% of multicryptal patches observed in sections of intestine from *Pms2^cre/cre*; *Apc^CKO/CKO* mice (Figure 2C) [11]. In fact, the *Pms2^cre/+*; *Apc^CKO/CKO* mice did not show any significant change in the number or size distribution of β-gal⁺ patches compared with *Pms2^cre/+*; *Apc^+/+* controls (Supplementary Table 2, available at *Carcinogenesis* Online). Interestingly, we observed a significant increase in the number of multicryptal β-gal⁺ foci with age (Figure 2D), suggesting that a low level of crypt fission persists in the adult intestine. Tumorigenesis was also much less evident in the *Pms2^cre/+* mice compared with *Pms2^cre/cre* mice. Even at ~2 years of age, *Pms2^cre/+*; *Apc^CKO/CKO* mice developed an average of only one intestinal adenoma. Tumorigenesis was rare in *Pms2^cre/+*; *Apc^CKO/CKO* β-gal⁺ foci, as less than 1% of β-gal⁺ foci were scored as microadenomas or adenomas in sections (1/176) or in wholemount (10/8387). In contrast, in *Pms2^cre/cre*; *Apc^CKO/CKO* mice, 17% (22/129) of β-gal⁺ foci were scored as either microadenomas or adenomas in sections ($P < 0.001$) (Figure 2C). To test the importance of later *Apc* loss in a background of *Apc*-heterozygosity, we generated *Pms2^cre/+*; *Apc^Δ/CKO* or *Pms2^cre/+*; *Apc^1638N/CKO* mice. We found that later loss of *Apc*, even in a background of *Apc*-heterozygosity, did not alter the size distribution of β-gal⁺ foci compared with *Pms2^cre/+* mice (Supplementary Table 2, available at *Carcinogenesis* Online) or increase the number of tumors compared with *Apc^Δ/+* or *Apc^1638N/+* mice, respectively (Supplementary Figure 6, available at *Carcinogenesis* Online), suggesting that a field of *Apc* deficiency is important, even in the setting of an inherited *Apc* mutation. Taken together, these results suggest that promotion of adenoma formation following *Apc* loss is much more probable earlier in life during intestinal growth because

Apc-deficient crypts have a greater chance of increased occult crypt fission.

Both Apc^{CKO} target alleles are efficiently recombined in β-gal$^+$ cells from Pms2$^{cre/+}$ mice

We showed previously that both *Apc*^{CKO} alleles were efficiently recombined in β-gal$^+$ normal and tumor tissue from *Pms2*$^{cre/cre}$ mice (11). Nevertheless, the relative lack of increased crypt fission and adenoma formation in *Pms2*$^{cre/+}$ mice could simply reflect inefficient Cre-mediated recombination of both *Apc* target alleles. To further test the efficiency of Cre recombination at *Apc*, we used either fluorescence-activated cell sorting of recombined (YFP$^+$) cells or laser capture microdissection samples coupled with PCR to genotype individual recombined (β-gal$^+$) foci.

For the laser capture microdissection-PCR, we calculated the ratio of the recombined *Apc* allele (*Apc*^{Δ}) to the unrecombined *Apc* allele (*Apc*^{CKO}) and compared the ratios to control samples, β-gal$^-$;*Apc*$^{CKO/CKO}$ or *Apc*$^{Δ/CKO}$. In *Pms2*$^{cre/+}$; *Apc*$^{CKO/CKO}$ mice, 75% (9/12) of normal-appearing β-gal$^+$ foci showed a similar ratio of *Apc*^{Δ}:*Apc*^{CKO} as tumor tissue (*Apc*$^{Δ/Δ}$, *P* = 0.83), but an increased ratio when compared with either β-gal$^-$ patches (*P* < 0.001) or control, heterozygous (*Apc*$^{Δ/CKO}$) tissue (*P* = 0.001) (Figure 3A). The increased *Apc*^{Δ}:*Apc*^{CKO} ratio in normal-appearing β-gal$^+$ foci compared with control *Apc*$^{Δ/CKO}$ samples strongly supports efficient recombination of both *Apc* alleles in a majority of β-gal$^+$ foci.

We also generated *Pms2*$^{cre/cre}$; *ROSA-lox-stop-lox-Yfp* mice for fluorescence-activated cell sorting of YFP$^+$ and YFP$^-$ cells from *Apc*$^{CKO/+}$ or *Apc*$^{CKO/CKO}$ mice. RNA isolated from each population was assayed for recombination, which results in deletion of *Apc* exon 14. We found that RNA from *Apc*$^{CKO/CKO}$; YFP$^+$ cells lacked signal for exon 14, while both *Apc*$^{CKO/CKO}$; YFP$^-$ and *Apc*$^{CKO/+}$; YFP$^+$ cells contained *Apc* exon 14 RNA (Figure 3B). These results demonstrated efficient Cre-mediated recombinational deletion of exon 14 of both *Apc* alleles in YFP$^+$ cells.

Apc-deficient field size potentiates tumor initiation independently of mismatch repair status

Potentially, the greater propensity for adenoma formation in *Pms2*$^{cre/+}$; *Apc*$^{CKO/CKO}$ mice compared with *Pms2*$^{cre/+}$; *Apc*$^{CKO/CKO}$ mice could be due to the higher level of background mutation in the MMR-deficient *Pms2*$^{cre/cre}$ mice. Indeed, mice heterozygous for the *Apc*^{min} mutation do in fact develop more adenomas in a MMR-deficient, *Pms2* null background (25). To compare the tumorigenic potential of isolated versus fields of *Apc*-deficient crypts independently of MMR status, we used the *Lgr5-CreER* mouse model (13) in combination with the conditional *Apc*^{CKO} allele. Using this mouse model, we varied the frequency and field size of *Apc*-deficient crypts by altering the dose of tamoxifen given at similar times. The use of this system eliminates any effects of MMR status, removes possible differences based on timing of *Apc* loss and generates fields of *Apc*-deficient crypts from independent, neighboring events.

We administered tamoxifen via intraperitoneal injection into mice at two doses, 2 mg/mouse (high) and 0.2 mg/mouse (low). The higher dose, similar to that used by other investigators (9), resulted in 9.8% β-gal$^+$ crypts, whereas the lower dose resulted in 2.3% β-gal$^+$ crypts (*P* = 0.0001) (Figure 4A). Furthermore, with the higher dose, 56% (41/74) of β-gal$^+$ foci were multicryptal, of which 21% (16/74) comprised at least four neighboring β-gal$^+$ crypts. In contrast, the lower dose produced only 13% (17/127) multicryptal β-gal$^+$ foci (*P* < 0.001), with only 0.8% (1/127) comprising at least four neighboring β-gal$^+$ crypts (*P* < 0.001) (Figure 4B). These results show that varying the tamoxifen dose alters both the frequency and field size of recombined crypts.

Next, we injected *Lgr5-CreER*; *Apc*$^{CKO/CKO}$ mice with two different doses of tamoxifen. We used PCR to show that the conditional *Apc* allele was efficiently recombined in the intestine of mice injected with either the low or high dose of tamoxifen (Figure 3C). Whereas mice receiving the higher dose developed an average of 204 adenomas

in the entire small intestine, we found that the lower dose tamoxifen resulted in an average of only seven tumors (*P* = 0.0002) (Figure 4C). Therefore, the lower tamoxifen dose resulted in a dramatic ~30-fold lower incidence of tumors while reducing the number of β-gal$^+$ crypts by only 4-fold and in turn increasing the proportion of isolated β-gal$^+$ crypts. Furthermore, by comparing the fold difference in β-gal$^+$ foci and tumors between the low and high dose, we estimate that three or more neighboring *Apc*-deficient crypts are needed for tumorigenesis (Figure 4D). Although the increased background mutation in the MMR-deficient *Pms2*$^{cre/cre}$; *Apc*$^{CKO/CKO}$ mice could have enhanced adenoma formation, results with MMR-proficient *Lgr5-CreER*; *Apc*$^{CKO/CKO}$ mice provide further evidence that the field size of *Apc*-deficient crypts is an important determinant for adenoma initiation.

We predicted that large fields of mutant *Apc*-deficient crypts characteristically generated 'de novo' by high-dose tamoxifen administration should predispose to polyclonal adenomas because such fields should include numerous independent *Apc* loss events. Therefore, we analyzed adenomas from *Lgr5-CreER*; *Apc*$^{580S/580S}$; *R26R-Confetti* mice 28 days after a single injection of high-dose tamoxifen (5 mg) (14). In these 'Confetti' mice, adenomas arising from a single mutant cell should express only a single color, whereas adenomas arising from multiple independent mutant cells should display multiple color markers. As predicted, we found that a majority of adenomas (11/14) exhibited more than one fluorescent marker, illustrating that adenomas were mostly polyclonal, forming from multiple neighboring mutant crypts (Figure 4E–G).

Early administration of sulindac reduces the increased crypt fission and adenoma formation associated with early Apc loss

Because our present and previous (11) studies revealed the importance of mutant crypt clonal expansion for fostering adenoma initiation, we determined the effects of sulindac (26) on this early stage of tumorigenesis. Sulindac is an NSAID that reduces adenoma numbers in humans and mice (26–28), with earlier exposure having an improved response (29). We administered sulindac to *Pms2*$^{cre/cre}$; *Apc*$^{CKO/CKO}$ mice (i) prior to conception—before any reversion events have occurred, (ii) at weaning—after early reversion events have occurred but before obvious adenoma formation or (iii) in the adult at 2 months of age—after most reversion events have occurred and adenomas have begun to form.

When sulindac was administered prior to conception via the mothers' drinking water and continued throughout life, the total number of β-gal$^+$ foci remained unchanged compared with untreated mice (*P* = 0.95), suggesting that sulindac did not noticeably eliminate *Apc*-mutant cells through apoptosis or alter the rate of *Cre* reversion. However, we did observe a reduction in the number of medium and large β-gal$^+$ foci in *Pms2*$^{cre/cre}$; *Apc*$^{CKO/CKO}$ mice (*P* = 0.01 and *P* = 0.001) to levels similar to *Pms2*$^{cre/cre}$; *Apc*$^{+/+}$ control mice, consistent with sulindac suppressing the increased crypt fission associated with early *Apc* loss (Figure 5D). Furthermore, we observed in tissue sections that the percentage of multicryptal β-gal$^+$ patches returned to levels seen in the untreated mice when sulindac treatment was started at conception (Supplementary Figure 7A, available at *Carcinogenesis* Online). To determine whether sulindac generally affected the rate of crypt fission or had a targeted effect on *Apc*-deficient crypt fission, we scored the number of β-gal-negative crypts undergoing fission in the *Pms2*$^{cre/cre}$; *Apc*$^{CKO/CKO}$ intestine. We found that sulindac had no detectable effect on the fission rate of *Apc*$^{+/+}$ crypts (Supplementary Figure 7B, available at *Carcinogenesis* Online). Similar to our findings for *Apc*$^{+/+}$ crypts, we found that treatment of *Pms2*$^{cre/cre}$; *Apc*$^{CKO/+}$ mice with sulindac had no effect on the size or number of β-gal$^+$, *Apc*$^{+/-}$ foci (Supplementary Figure 5, available at *Carcinogenesis* Online). Taken together, our results strongly suggest that crypt fission inhibition by sulindac was specific to *Apc*-deficient crypts. In addition to the suppressive effect on *Apc*-deficient crypt fission, sulindac treatment initiated prior to conception resulted in a 3-fold decrease in adenomas compared with untreated *Pms2*$^{cre/cre}$; *Apc*$^{CKO/CKO}$ mice (*P* < 0.001) (Figure 5D). The inhibition by sulindac of both increased
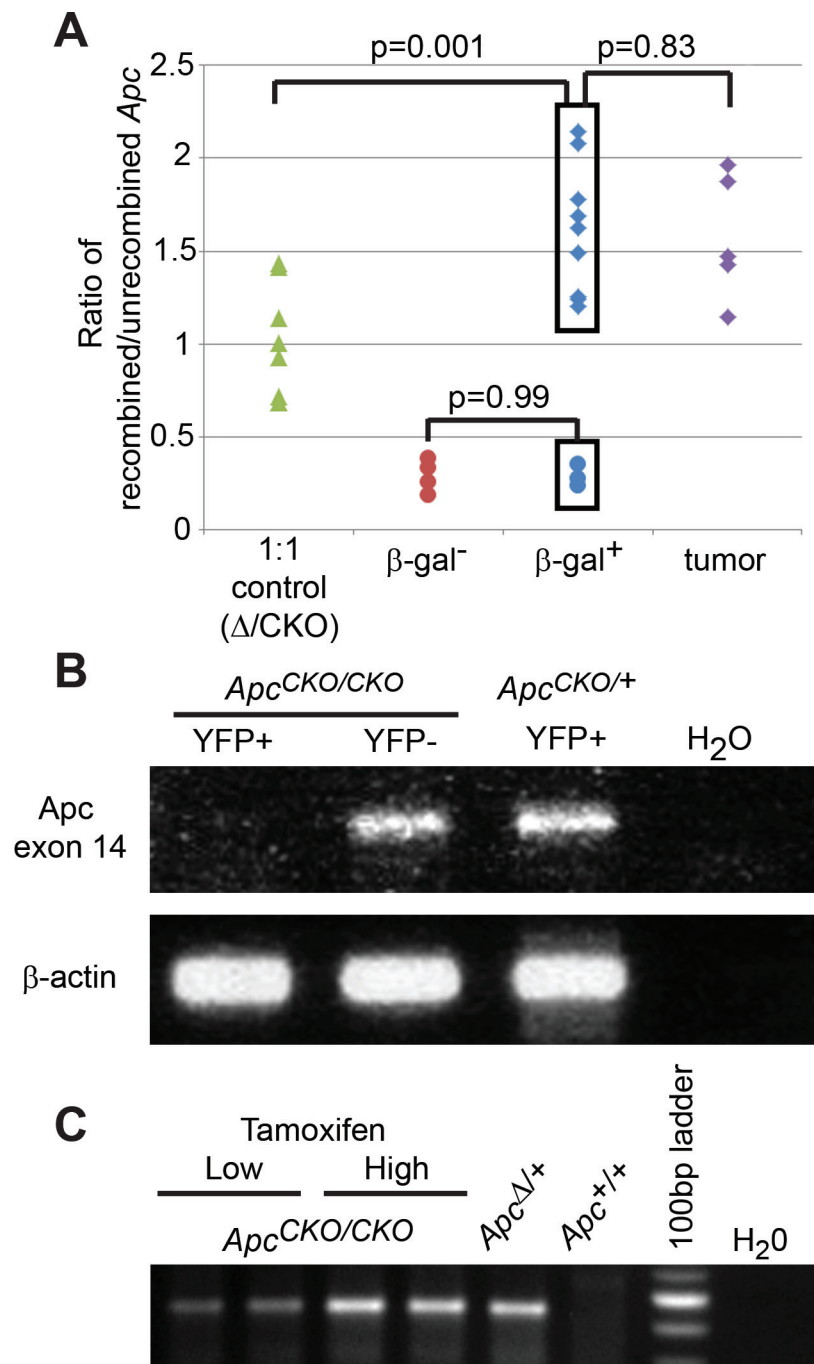
Fig. 3. Efficient recombination of Apc^{CKO} in $Pms2^{cre}$ and $Lgr5$-$CreER$ intestines. (**A**) Laser capture microdissection-PCR was used on isolated β-gal⁺ foci to detect the recombined Apc allele (Apc^{Δ}) and unrecombined Apc allele (Apc^{CKO}). DNA from $Pms2^{+/+}$; $Apc^{\Delta/CKO}$ mice, which contains equal amounts of Apc^{CKO} and Apc^{Δ} (1:1 control), was given an average ratio of 1 and used to normalize all experimental samples. Therefore, a ratio >1 shows a population of cells with more of the Apc^{Δ} alleles, while a ratio of <1 shows a population of cells with more of the Apc^{CKO} alleles. Tumors (purple diamonds) and 75% of the normal-appearing β-gal⁺ foci (blue diamonds) had a similar ratio of Apc^{Δ} to Apc^{CKO}, while the same β-gal⁺ foci had an increased ratio compared with either the β-gal⁻ foci (red circles) or control, heterozygous ($Apc^{\Delta/CKO}$) samples (green triangles). (**B**) Fluorescence-activated cell sorting was used to isolate 1000 YFP⁺ and YFP⁻ cells from crypts of either $Pms2^{cre/cre}$; $Apc^{CKO/CKO}$ or $Pms2^{cre/cre}$; $Apc^{CKO/+}$ intestine. RNA was isolated from the different populations and then analyzed for the presence of the floxed Apc exon (exon 14). The floxed exon was lost in YFP⁺; $Apc^{CKO/CKO}$ cells, but not in YFP⁻; $Apc^{CKO/CKO}$ or YFP⁺; $Apc^{CKO/+}$ cells. β-actin was used as a control. (**C**) PCR was used to detect the recombined Apc allele in intestinal sections from $Lgr5$-$CreER$; $Apc^{CKO/CKO}$ mice injected with either the high or low dose of tamoxifen. Apc was recombined in both treatments. More importantly, the 3.6-fold increase in recombined Apc DNA with high-dose treatment was in agreement with the observed 4-fold increase in β-gal⁺ crypts (see Figure 4A).

crypt fission and adenoma formation suggests a direct relationship and reinforces the idea that a field of Apc-deficient crypts is conducive to adenoma formation.

In stark contrast to 'preconception' administration, sulindac treatment initiated at weaning had no effect on the increased crypt fission

associated with Apc loss, as evidenced by no significant reduction in the number of medium and large β-gal⁺ foci compared with untreated mice ($P = 0.82$ and $P = 0.94$) (Figure 5D). Presumably, the growth advantage of $Apc^{-/-}$ crypts had already manifested prior to weaning. However, we did observe a slight reduction in adenoma number
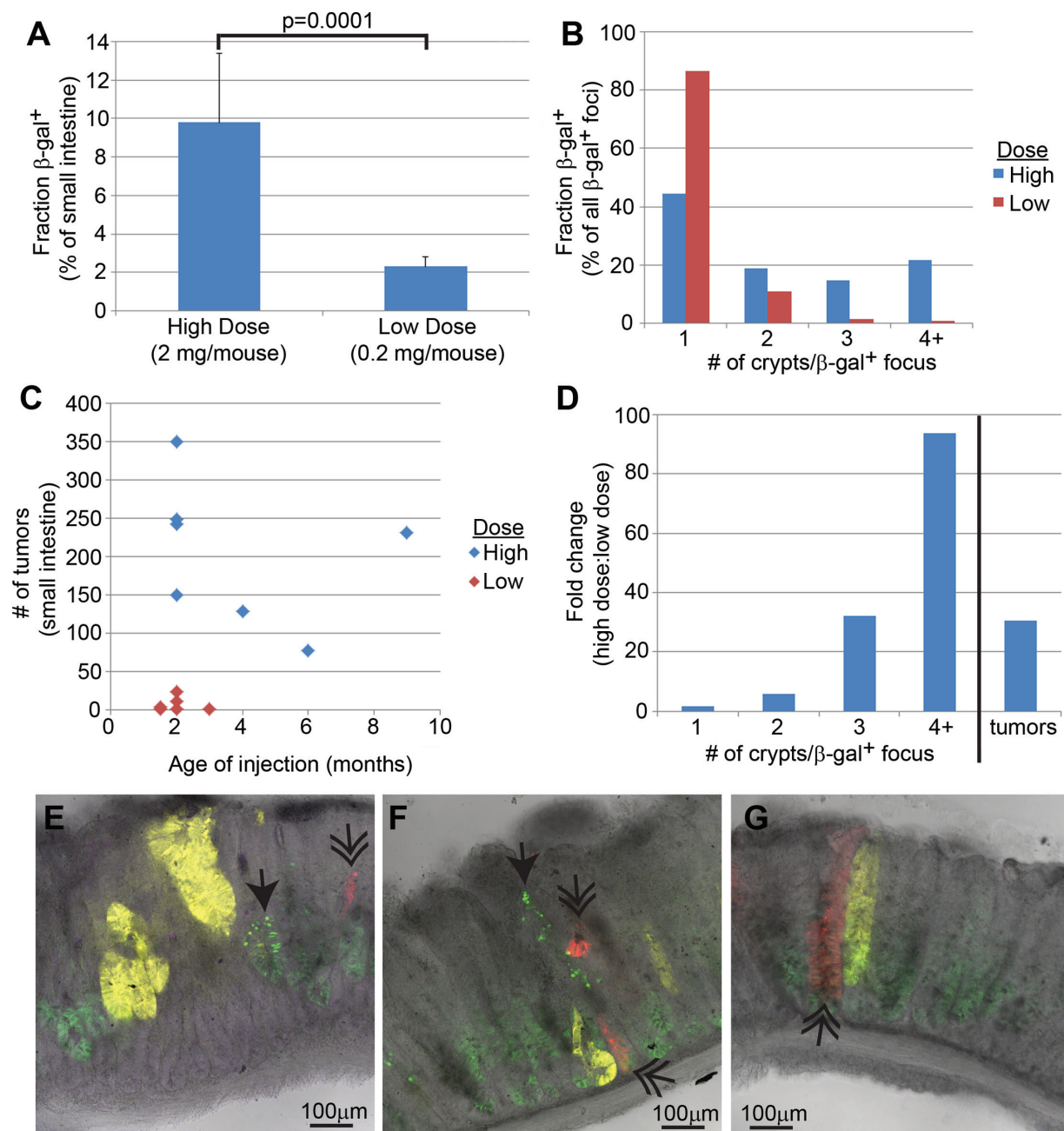
Fig. 4. Characterization of recombination in *Lgr5-CreER* mice. (**A**) A 4-fold difference between the high (*n* = 4) and low (*n* = 8) dose of tamoxifen in the percentage of tissue with marker gene recombination. (**B**) The increased β-gal⁺ focus size in the intestine following high-dose tamoxifen as measured by the number of neighboring β-gal⁺ crypts. (**C**) The increased number of tumors in *Lgr5-CreER*; *Apc^{CKO/CKO}* intestine following high-dose tamoxifen. (**D**) The higher dose of tamoxifen gives a higher ratio of larger β-gal⁺ fields. As discussed in the text, we estimate that at least three neighboring crypts are required for efficient adenoma initiation. (**E–G**) Images of adenomas from an *Lgr5-CreER*; *Apc^{580S/580S}*; *R26R-Confetti* mouse injected with a single, high dose of tamoxifen. Notice the multiple different fluorescent proteins found in single adenomas [nuclear green fluorescent protein (single arrowhead), red fluorescent protein (double arrowhead) and yellow fluorescent protein]. Cytoplasmic green fluorescent protein is from the Lgr5-targeted transgene.

(*P* = 0.02) (Figure 5D). Sulindac treatment initiated at 2 months of age failed to alter either the size distribution of normal-appearing *Apc*-deficient crypts (*P* = 0.99 and *P* = 0.39) or reduce adenoma number when compared with untreated mice (*P* = 0.93) (Figure 5D). These data show that similar to prior studies (29), sulindac is most effective in reducing adenoma formation when administered early. In addition, sulindac does not appear to act only by eliminating *Apc*-deficient cells via increased apoptosis. Rather, our results suggest that sulindac can also reduce adenoma number by inhibiting the accelerated crypt fission associated with *Apc* loss and is most effective in reducing the tumor burden when *Apc*-mutant field size is minimized. Taken

together, the sulindac results combined with the *Pms2^{cre}* and *Lgr5-CreER* data above suggest that adenomas arise most efficiently from a field of *Apc*-mutant crypts, which can form from either occult crypt fission or independent, neighboring events.

Discussion

In the current study, we have exploited Cre/*lox* systems in the mouse to alter *Apc* in the intestine. From our results, we offer some novel conclusions concerning intestinal tumor initiation and prevention. Specifically: (i) Sporadic *Apc* loss in single isolated cells does not
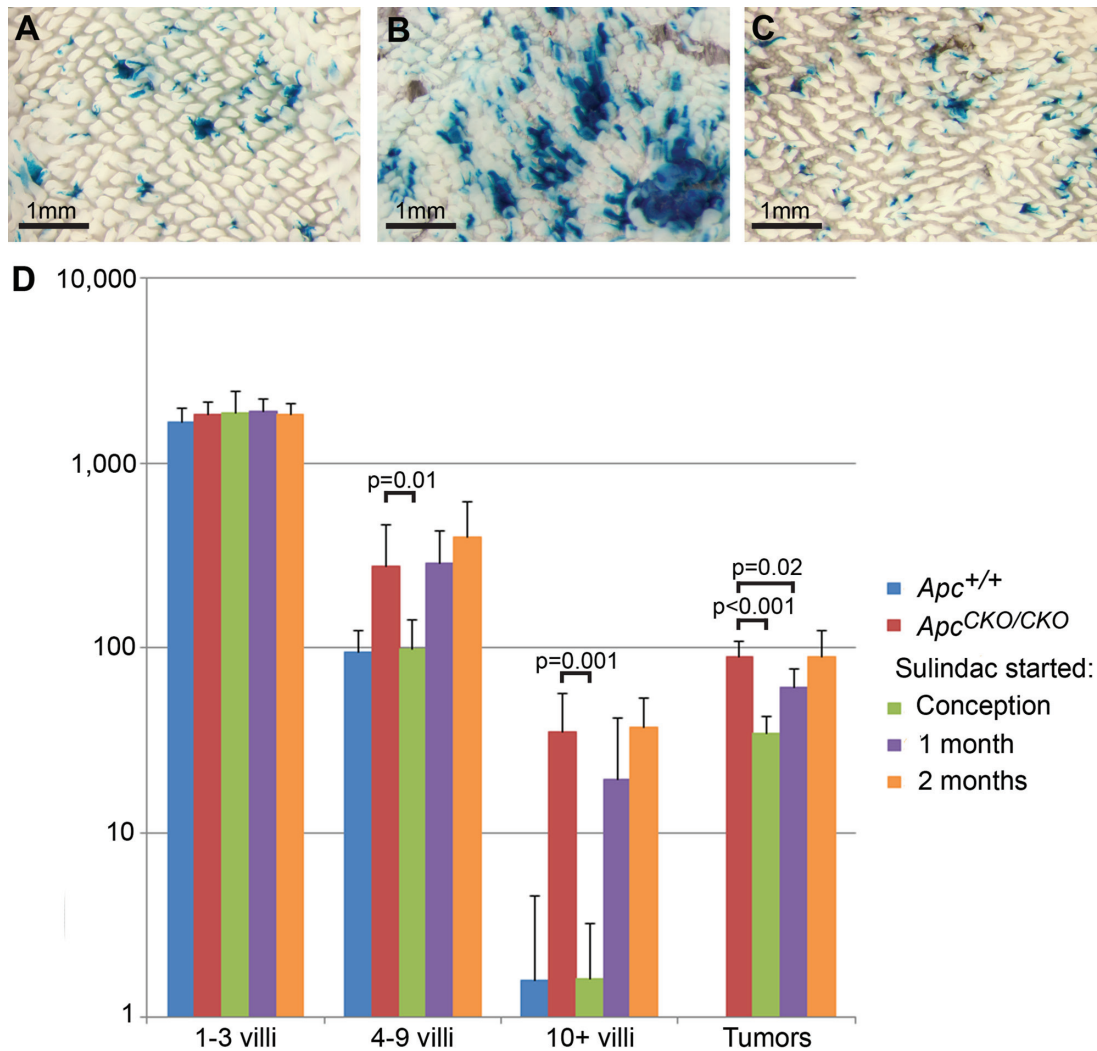
Fig. 5. Effects of sulindac treatment on crypt fission and adenoma formation in *Pms2$^{cre/cre}$* mice. *Pms2$^{cre/cre}$*; *Apc$^{+/+}$* (**A**), *Pms2$^{cre/cre}$*; *Apc$^{CKO/CKO}$* (**B**) and *Pms2$^{cre/cre}$*; *Apc$^{CKO/CKO}$* (**C**) mice administered sulindac continuously from conception. Note the striking increase in β-gal$^+$ focus size when comparing *Pms2$^{cre/cre}$*; *Apc$^{+/+}$* (A) and *Pms2$^{cre/cre}$*; *Apc$^{CKO/CKO}$* mice (B) versus the obvious similarity between the β-gal$^+$ focus sizes in the sulindac-treated intestine (C) and the control intestine (A). (**D**) β-gal$^+$ foci and tumor numbers in *Pms2$^{cre/cre}$* control mice ($n = 7$) and *Pms2$^{cre/cre}$*; *Apc$^{CKO/CKO}$* mice untreated ($n = 6$) or treated with sulindac started at conception ($n = 8$), 1 month ($n = 6$) or 2 months ($n = 3$). Sulindac treatment started prior to conception, via the mother's drinking water, resulted in a significant decrease in medium (4–9 villi) and large (10+ villi) β-gal$^+$ foci and tumor number compared with untreated *Apc$^{CKO/CKO}$* mice. Sulindac started at weaning (1 month) resulted in a significant decrease in tumor number, but not β-gal$^+$ focus size. Sulindac started in adult mice at 2 months had no significant effect on β-gal$^+$ focus size or tumor number. Total β-gal$^+$ foci numbers and tumor numbers were determined in wholemount.

usually change morphologic phenotype, with most *Apc$^{-/-}$* cells residing in normal-appearing crypts. (ii) Early *Apc* loss results in increased crypt fission that in turn enhances adenoma formation. (iii) The observed phenotypic plasticity of *Apc*-deficient crypts is regulated by field size, with larger field size fostering adenoma formation. (iv) Sulindac can suppress tumor formation by inhibiting the increased occult crypt fission of *Apc*-deficient cells.

Rather than 'instantaneous' transformation and a direct correlation between genotype and phenotype, our studies revealed considerable phenotypic plasticity with the majority of *Apc*-deficient single crypts retaining normal morphologic phenotypes. Although *Apc* is a driver mutation, we suggest that the local environment can influence the phenotype in *Apc*-deficient crypts. For example, the genome from a fully transformed melanoma cell can be completely 'reprogrammed' by nuclear transfer and contribute to the formation of a normal mouse (30). However, we do show that *Apc*-mutant crypts are functionally abnormal because they can exhibit accelerated crypt fission, as manifested by increased numbers of larger mutant patches. Moreover, these advantages are more highly expressed during early development when intestinal growth by crypt fission is ongoing and

mutant crypts can more readily outcompete normal crypts (31). Once intestinal growth has slowed in the adult mouse, most phenotypically normal *Apc*-deficient cells have a reduced chance of displacing surrounding normal crypts because most mutant patches remain isolated. This observation is consistent with data from *Apc$^{Min/+}$* mice demonstrating that carcinogens administered early in life produce the highest numbers of adenomas (32). Our data add to this concept and illustrate how early mutations are inherently better able to spread due to the normal crypt fission that occurs during growth.

We have utilized the MMR status of *Pms2^{cre}* mice to alter the frequency and time frame of *Cre* reversion. Compromised MMR in *Pms2$^{cre/cre}$* mice will result in both increased *Cre* reversion and a higher mutation rate throughout the genome. However, while an increased mutation rate could complicate our observations, we offer several reasons for why our data are not hindered by *Pms2* deficiency. First, we compare *Pms2*-deficient experimental mice harboring floxed target genes with *Pms2*-deficient control mice that lack targets. Second, we analyze hundreds of reversion events per mouse, thus the stochastic nature of any 'background' mutations makes modifying a consequential gene in a significant fraction of β-gal$^+$ foci highly

unlikely. Furthermore, *Pms2*-null mice are not prone to either intestinal adenomas or carcinomas (33). Although we cannot rule out some undefined synergistic effect between the Cre targeted mutations and *Pms2* deficiency, we believe such an effect is highly unlikely to play a significant role in influencing the phenotypes of Cre-expressing cells in *Pms2^{cre/cre}* mice.

The idea that fields of mutant crypts can promote tumorigenesis was proposed previously to explain polyclonal adenomas often found in mice and humans heterozygous for *Apc* mutation (5,15,16). Furthermore, tumor polyclonality was explained by short-range interactions between neighboring mutant crypts (34). In contrast, other studies showed that intestinal adenomas could also be monoclonal and thus derived from single crypts (35). Our data using the *Pms2^{cre}* system indicated that a field of *Apc*-deficient crypts originated in a single crypt followed by occult crypt fission. In addition, our results using the inducible *Lgr5-CreER* system showed that multiple independent, neighboring events can also produce a field that is conducive to the formation of polyclonal adenomas. Our analysis suggests that a field of at least three crypts is necessary for tumorigenesis. Therefore, we propose that adenomas can initiate by occult crypt fission and/or independent, neighboring events. Taken together, our results suggest that *Apc*-mutant fields, regardless of how formed, are conducive to adenoma formation. While our data are focused on intestinal cancer and *Apc* mutation, field effects have also been reported for other genes/cancers, such as *p53* in esophageal cancer (6), ulcerative colitis-associated neoplasia (7) and *Cdh3* in colorectal cancer (8). Field effects can manifest in a variety of ways, such as transcriptional and proliferative changes in benign prostate from prostate cancer patients (36,37), metabolic changes in non-dysplastic tissue from esophageal cancer patients (38) and methylation defects in the colonic mucosa from colorectal cancer patients (39).

A phenotypically normal phase of mutant cells before tumorigenesis has important implications for human cancer progression. First, the lack of visible adenomas early in life in mice and humans with heterozygous germline *Apc* mutations is difficult to explain if adenoma formation requires a simple loss of the normal *Apc* allele in a single stem cell. Based on our findings, we propose that loss of the functional *Apc* allele regularly occurs but that phenotypic plasticity allows *Apc*-deficient mutant crypts arising early in life to accumulate and only subsequently evolve into adenomas during adolescence. For example, in familial adenomatous polyposis patients there are hundreds of visible monocryptal lesions that seem to progress through crypt fission (40). Our data suggest that an even earlier stage in adenoma initiation

is a phenotypically normal, but *Apc*-deficient crypt, which can remain normal for an extended length of time until a field of *Apc*-deficient crypts arises. Second, the large number of passenger mutations in human colorectal cancers implies that many mutations accumulate in normal intestine (41). Indeed, it has been estimated that over half of all the mutations in a cancer accumulated in normal colon tissue (41–43). Phenotypic plasticity facilitates the accumulation of both driver and passenger mutations throughout life as opposed to a simple stepwise progression, in which driver mutations accumulate only in visible tumors.

Because our studies with the *Pms2^{cre}* mice revealed the importance of mutant crypt clonal expansion for fostering adenoma initiation, we sought to determine the effects of a chemopreventive on this early stage before tumor progression. Sulindac is an NSAID that reduces adenoma numbers in humans and mice (26–29). Previous data from mice have led investigators to postulate that sulindac acts via stimulating apoptosis of *Apc*-deficient stem cells (44). Such an apoptotic mechanism should result in a marked reduction in β-gal^+; *Apc*-deficient foci in our system. However, we found that the numbers of normal-appearing β-gal^+; *Apc^{−/−}* foci were similar between treated and untreated mice. Interestingly, however, sulindac treatment resulted in smaller β-gal^+; *Apc^{−/−}* foci. Therefore, we suggest that sulindac reduces adenoma numbers in the mouse not only by increasing apoptosis within the adenoma, as shown convincingly by previous investigators (44), but also by limiting the increased crypt fission and subsequent mutant field formation associated with *Apc* loss. Sulindac may therefore block the gatekeeper function of *Apc* deficiency or the net increase in mutant cells. Elucidating the mechanism by which sulindac can inhibit increased crypt fission associated with *Apc* loss is worthy of further investigation.

In terms of human cancer prevention, low-dose NSAID (e.g. aspirin) use has been associated with significantly reduced colorectal cancer risk (45), most often explained by increased apoptosis of *Apc*-deficient cells (46–48). However, reductions in cancer risk require 5 or more years of aspirin use (49), and the chronicity of use rather than the dosage appears to be critical for prevention (50). These epidemiologic findings are difficult to explain if the only chemopreventive mechanism is by apoptotic elimination of mutant cells. An additional explanation, based on our findings with sulindac reported here, is that chronic low-dose NSAIDs limit the expansion of *Apc*-deficient cells, therefore reducing tumorigenesis by inhibiting the otherwise enhanced crypt fission of *Apc*-mutant cells (51–53). As reported for
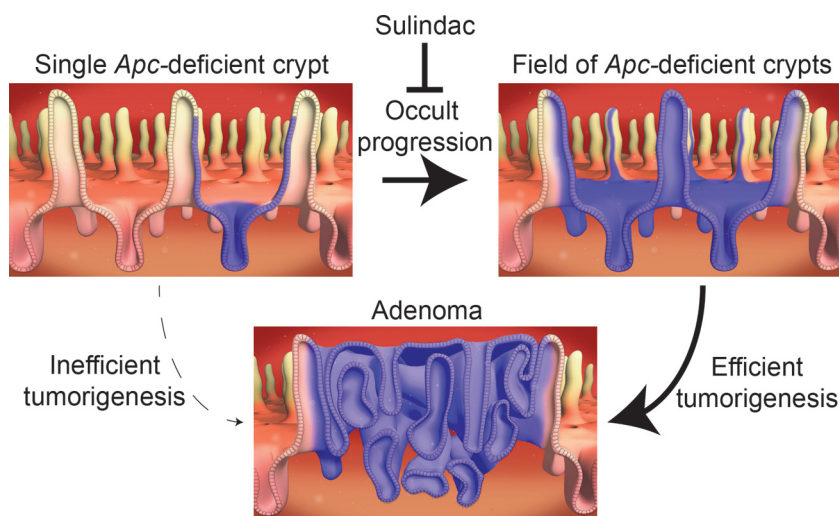

Fig. 6. Model for progression from an isolated *Apc*-deficient crypt to adenoma. First, an isolated stem cell loses *Apc* function during development of the intestine. Next, the *Apc*-mutant stem cell spreads by crypt succession to monoclonality. Possessing a selective advantage, the *Apc*-deficient crypt forms a field of mutant crypts via increased crypt fission. A field of *Apc*-deficient crypts is now primed to undergo tumorigenesis and produce an adenoma. Finally, sulindac blocks the crypt fission advantage of *Apc*-deficient crypts, thus preventing a field of mutant crypts from forming and hence tumorigenesis. Sulindac seems to have minimal effect on tumorigenesis after the field of *Apc*-deficient crypts has formed.

adult humans (8,54), we observed continued crypt fission in adult mice (Figure 2D), albeit at a slower rate than during development (31,55). Because a low level of crypt fission persists in the adult, the possibility remains that new sporadic *Apc* mutations can accumulate in isolated crypts and over years create small fields of mutant crypts. The reduction in tumors after chronic aspirin use in humans could reflect the inhibition of the enhanced crypt fission of *Apc*-deficient crypts observed with sulindac in this study. This inhibition would reduce, but not completely prevent, any new field expansions of *Apc*-deficient crypts. In addition, fields of *Apc*-deficient crypts that were already established would not be eliminated. Therefore, we believe that our data can help explain why low-dose aspirin does not immediately reduce cancer risks, does not completely eliminate the chance of getting a tumor and requires at least 5 years of chronic administration to reduce the chance of cancer by 30–40% (45,56).

In summary, the ability to engineer and follow the fates of specific sporadic mutations in marked single cells has revealed both the phenotypic plasticity of *Apc*-mutant intestinal cells and the subsequent occult clonal expansion of mutant crypts via increased crypt fission. Such increased crypt clonal expansion by normal-appearing *Apc*-deficient crypts is consistent with the gatekeeper role of *Apc* but occurs without the microscopic or macroscopic manifestations of adenomas. Instead of a simple linear progression to cancer with genotype intrinsically associated with morphologic phenotype, our system reveals that the timing of mutation can influence morphologic phenotype, crypt fission and adenoma progression. Mutations can hitchhike and augment the crypt fission that occurs during normal growth and development. Most notably, the formation of a field of mutant crypts appears to be a more efficient tumor initiation pathway compared with the same mutations that remain isolated in single crypts. In addition, we find that limiting *Apc*-deficient occult crypt fission can serve as a previously unappreciated mechanism of chemoprevention (Figure 6).

Supplementary material

Supplementary methods and Supplementary Tables 1 and 2 and Figures 1–7 can be found at http://carcin.oxfordjournals.org/

Funding

Acknowledgements

Conflict of Interest Statement: H.C. is an inventor of several patents involving the organoid culture system. The remaining authors disclose no conflicts.

References

1. Vogelstein,B. *et al.* (1985) Use of restriction fragment length polymorphisms to determine the clonal origin of human tumors. *Science*, **227**, 642–645.
2. Network,T.C.G.A. (2012) Comprehensive molecular characterization of human colon and rectal cancer. *Nature*, **487**, 330–337.
3. Garcia,S.B. *et al.* (1999) Field cancerization, clonality, and epithelial stem cells: the spread of mutated clones in epithelial sheets. *J. Pathol.*, **187**, 61–81.
4. Shen,L. *et al.* (2005) MGMT promoter methylation and field defect in sporadic colorectal cancer. *J. Natl Cancer Inst.*, **97**, 1330–1338.
5. Thliveris,A.T. *et al.* (2005) Polyclonality of familial murine adenomas: analyses of mouse chimeras with low tumor multiplicity suggest short-range interactions. *Proc. Natl Acad. Sci. USA*, **102**, 6960–6965.
6. Prevo,L.J. *et al.* (1999) p53-mutant clones and field effects in Barrett's esophagus. *Cancer Res.*, **59**, 4784–4787.
7. Leedham,S.J. *et al.* (2009) Clonality, founder mutations, and field cancerization in human ulcerative colitis-associated neoplasia. *Gastroenterology*, **136**, 542–550.e6.
8. Milicic,A. *et al.* (2008) Ectopic expression of P-cadherin correlates with promoter hypomethylation early in colorectal carcinogenesis and enhanced intestinal crypt fission *in vivo*. *Cancer Res.*, **68**, 7760–7768.
9. Barker,N. *et al.* (2009) Crypt stem cells as the cells-of-origin of intestinal cancer. *Nature*, **457**, 608–611.
10. Clarke,A.R. (2005) Studying the consequences of immediate loss of gene function in the intestine: APC. *Biochem. Soc. Trans.*, **33**(Pt 4), 665–666.
11. Fischer,J.M. *et al.* (2012) Different phenotypic consequences of simultaneous versus stepwise Apc loss. *Oncogene*, **31**, 2028–2038.
12. Kwong,L.N. *et al.* (2009) APC and its modifiers in colon cancer. *Adv. Exp. Med. Biol.*, **656**, 85–106.
13. Barker,N. *et al.* (2007) Identification of stem cells in small intestine and colon by marker gene Lgr5. *Nature*, **449**, 1003–1007.
14. Schepers,A.G. *et al.* (2012) Lineage tracing reveals Lgr5+ stem cell activity in mouse intestinal adenomas. *Science*, **337**, 730–735.
15. Thliveris,A.T. *et al.* (2011) Clonal structure of carcinogen-induced intestinal tumors in mice. *Cancer Prev. Res. (Phila).*, **4**, 916–923.
16. Novelli,M.R. *et al.* (1996) Polyclonal origin of colonic adenomas in an XO/XY patient with FAP. *Science*, **272**, 1187–1190.
17. Kuraguchi,M. *et al.* (2006) Adenomatous polyposis coli (APC) is required for normal development of skin and thymus. *PLoS Genet.*, **2**, e146.
18. Zambrowicz,B.P. *et al.* (1997) Disruption of overlapping transcripts in the ROSA beta geo 26 gene trap strain leads to widespread expression of beta-galactosidase in mouse embryos and hematopoietic cells. *Proc. Natl Acad. Sci. USA*, **94**, 3789–3794.
19. Snippert,H.J. *et al.* (2010) Intestinal crypt homeostasis results from neutral competition between symmetrically dividing Lgr5 stem cells. *Cell*, **143**, 134–144.
20. Sato,T. *et al.* (2009) Single Lgr5 stem cells build crypt-villus structures *in vitro* without a mesenchymal niche. *Nature*, **459**, 262–265.
21. Miller,A.J. *et al.* (2008) Tractable Cre-lox system for stochastic alteration of genes in mice. *Nat. Methods*, **5**, 227–229.
22. Sangiorgi,E. *et al.* (2008) Bmi1 is expressed *in vivo* in intestinal stem cells. *Nat. Genet.*, **40**, 915–920.
23. Fischer,J.M. *et al.* (2008) Visualizing loss of heterozygosity in living mouse cells and tissues. *Mutat. Res.*, **645**, 1–8.
24. Sato,T. *et al.* (2011) Paneth cells constitute the niche for Lgr5 stem cells in intestinal crypts. *Nature*, **469**, 415–418.
25. Baker,S.M. *et al.* (1998) Enhanced intestinal adenomatous polyp formation in Pms2-/-;Min mice. *Cancer Res.*, **58**, 1087–1089.
26. Boolbol,S.K. *et al.* (1996) Cyclooxygenase-2 overexpression and tumor formation are blocked by sulindac in a murine model of familial adenomatous polyposis. *Cancer Res.*, **56**, 2556–2560.
27. Waddell,W.R. *et al.* (1983) Sulindac for polyposis of the colon. *J. Surg. Oncol.*, **24**, 83–87.
28. Giardiello,F.M. *et al.* (1993) Treatment of colonic and rectal adenomas with sulindac in familial adenomatous polyposis. *N. Engl. J. Med.*, **328**, 1313–1316.
29. Beazer-Barclay,Y. *et al.* (1996) Sulindac suppresses tumorigenesis in the Min mouse. *Carcinogenesis*, **17**, 1757–1760.
30. Hochedlinger,K. *et al.* (2004) Reprogramming of a melanoma genome by nuclear transplantation. *Genes Dev.*, **18**, 1875–1885.
31. Cheng,H. *et al.* (1985) Whole population cell kinetics and postnatal development of the mouse intestinal epithelium. *Anat. Rec.*, **211**, 420–426.
32. Shoemaker,A.R. *et al.* (1995) N-ethyl-N-nitrosourea treatment of multiple intestinal neoplasia (Min) mice: age-related effects on the formation of intestinal adenomas, cystic crypts, and epidermoid cysts. *Cancer Res.*, **55**, 4479–4485.
33. Prolla,T.A. *et al.* (1998) Tumour susceptibility and spontaneous mutation in mice deficient in Mlh1, Pms1 and Pms2 DNA mismatch repair. *Nat. Genet.*, **18**, 276–279.
34. Halberg,R.B. *et al.* (2007) Polyclonal tumors in the mammalian intestine: are interactions among multiple initiated clones necessary for tumor initiation, growth, and progression? *Cell Cycle*, **6**, 44–51.
35. Fearon,E.R. *et al.* (1987) Clonal analysis of human colorectal tumors. *Science*, **238**, 193–197.
36. Kosari,F. *et al.* (2012) Shared gene expression alterations in prostate cancer and histologically benign prostate from patients with prostate cancer. *Am. J. Pathol.*, **181**, 34–42.
37. Ananthanarayanan,V. *et al.* (2006) Alteration of proliferation and apoptotic markers in normal and premalignant tissue associated with prostate cancer. *BMC Cancer*, **6**, 73.

38. Yakoub,D. *et al.* (2010) Metabolic profiling detects field effects in non-dysplastic tissue from esophageal cancer patients. *Cancer Res.*, **70**, 9129–9136.

39. Svrcek,M. *et al.* (2010) Methylation tolerance due to an O6-methylguanine DNA methyltransferase (MGMT) field defect in the colonic mucosa: an initiating step in the development of mismatch repair-deficient colorectal cancers. *Gut*, **59**, 1516–1526.

40. Preston,S.L. *et al.* (2003) Bottom-up histogenesis of colorectal adenomas: origin in the monocryptal adenoma and initial expansion by crypt fission. *Cancer Res.*, **63**, 3819–3825.

41. Tomasetti,C. *et al.* (2013) Half or more of the somatic mutations in cancers of self-renewing tissues originate prior to tumor initiation. *Proc. Natl Acad. Sci. USA*, **110**, 1999–2004.

42. Calabrese,P. *et al.* (2004) Colorectal pretumor progression before and after loss of DNA mismatch repair. *Am. J. Pathol.*, **164**, 1447–1453.

43. Calabrese,P. *et al.* (2004) Pretumor progression: clonal evolution of human stem cell populations. *Am. J. Pathol.*, **164**, 1337–1346.

44. Qiu,W. *et al.* (2010) Chemoprevention by nonsteroidal anti-inflammatory drugs eliminates oncogenic intestinal stem cells via SMAC-dependent apoptosis. *Proc. Natl Acad. Sci. USA*, **107**, 20027–20032.

45. Rothwell,P.M. (2013) Aspirin in prevention of sporadic colorectal cancer: current clinical evidence and overall balance of risks and benefits. *Recent Results Cancer Res.*, **191**, 121–142.

46. Stark,L.A. *et al.* (2007) Aspirin activates the NF-kappaB signalling pathway and induces apoptosis in intestinal neoplasia in two *in vivo* models of human colorectal cancer. *Carcinogenesis*, **28**, 968–976.

47. Ashktorab,H. *et al.* (2005) Apoptosis induced by aspirin and 5-fluorouracil in human colonic adenocarcinoma cells. *Dig. Dis. Sci.*, **50**, 1025–1032.

48. Yoshikawa,R. *et al.* (1995) Effect of aspirin on the induction of apoptosis in colorectal adenocarcinoma cell-lines. *Oncol. Rep.*, **2**, 361–364.

49. Rothwell,P.M. *et al.* (2012) Short-term effects of daily aspirin on cancer incidence, mortality, and non-vascular death: analysis of the time course of risks and benefits in 51 randomised controlled trials. *Lancet*, **379**, 1602–1612.

50. Rothwell,P.M. *et al.* (2010) Long-term effect of aspirin on colorectal cancer incidence and mortality: 20-year follow-up of five randomised trials. *Lancet*, **376**, 1741–1750.

51. Wasan,H.S. *et al.* (1998) APC in the regulation of intestinal crypt fission. *J. Pathol.*, **185**, 246–255.

52. Bjerknes,M. *et al.* (1997) APC mutation and the crypt cycle in murine and human intestine. *Am. J. Pathol.*, **150**, 833–839.

53. Bjerknes,M. (1996) Expansion of mutant stem cell populations in the human colon. *J. Theor. Biol.*, **178**, 381–385.

54. Totafurno,J. *et al.* (1987) The crypt cycle. Crypt and villus production in the adult intestinal epithelium. *Biophys. J.*, **52**, 279–294.

55. Cummins,A.G. *et al.* (2008) Crypt fission peaks early during infancy and crypt hyperplasia broadly peaks during infancy and childhood in the small intestine of humans. *J. Pediatr. Gastroenterol. Nutr.*, **47**, 153–157.

56. Rothwell,P.M. *et al.* (2011) Effect of daily aspirin on long-term risk of death due to cancer: analysis of individual patient data from randomised trials. *Lancet*, **377**, 31–41.